ISSN 1392–1320 MATERIALS SCIENCE (MEDŽIAGOTYRA). Vol. 29, No. 4. 2023

Microstructure and Mechanical Properties of Fe-Based Alloy Coatings Fabricated by Laser Cladding

Lu XIE [1]*, Yueming WANG [2]

[1] *School of Management Engineering, Jiangsu Urban and Rural Construction Vocational College, Changzhou 213147, China*
[2] *Hunan Provincial Key Defense Laboratory of High Temperature Wear-resisting Materials and Preparation Technology, Hunan University of Science and Technology, Xiangtan 411201, PR China*

http://doi.org/10.5755/j02.ms.33919

Received 27 April 2023; accepted 25 May 2023

The Fe-based alloy coating was prepared on the surface of 25Cr2Ni4MoV steel substrate by laser cladding. The microstructure, microhardness, shear strength, friction and wear properties of the laser cladding coating were systematically studied. The results show that a good metallurgical bond has been formed between Fe-based alloy coating and substrate. The laser cladding layer is a typical dendritic crystal, which is composed of light gray and dark gray phases. The shear strength displacement curve shows the typical characteristics of brittle fracture, with an average shear strength of 280.83 MPa. The average dry friction coefficient, wear track depth and average wear volume of laser cladding Fe-based alloy coatings are (0.45 ± 0.01), (26 ± 3) μm and 0.066615 m^3, respectively. The average dry friction coefficient, wear track depth and average wear volume of 25Cr2Ni4MoV substrate are (0.60 ± 0.01), (39 ± 3) μm and 0.13085 m^3, respectively. The laser cladded Fe-based alloy coating exhibits much better wear resistance than the steel substrate, and the shear strength of the coating displays its potential for the application in the service environment of shear stress.

Keywords: laser cladding, Fe-based alloy, coating, microstructure, mechanical properties.

1. INTRODUCTION

Laser cladding is an advanced coating technology that simultaneously melts powder and substrate surface and coats the melted powder into the substrate melting pool, then the powder will solidify into the coating. Laser cladding technology obtains many advantages as high coating density, high bonding strength and fast fabrication, relative to traditional coating technologies like thermal spray, cold spray, PVD, CVD and so on [1 – 6].

Metal alloy powder, like Fe-based, Ni-based and Co-based alloy, is usually adopted as the raw material for laser cladding. Among these kinds of powder, Fe-based alloy powder has been researched on wear-resistant coating fabrication more and more, due to its high hardness, high wear resistance and relatively low cost. Lu et al. [7] investigated the effect of WC content on the microstructure and wear resistance of laser cladded Fe-based alloy coating. The result showed that the friction coefficient of Fe-based alloy coating gradually decreased and the wear resistance was improved with the addition of WC. Luo et al. [8] fabricated Fe-Al alloy coating on 1045 steel by laser cladding, using the alloy powder which was treated by high-energy ball milling. The result showed the friction coefficient was 0.64, and the wear rate was 0.3251×10^{-3} $mm^3 \cdot N^{-1} \cdot m^{-1}$. Zhao et al. [9] obtained Fe-Al-Si coating by laser cladding, and investigated the effects of laser power and scanning velocity on coating properties. They found that as the power and scanning velocity increased, the grain size gradually decreased, the hardness and wear resistance were constantly improved. The optimal laser power and scanning velocity were 1600 W and 400 mm/min, respectively. Ju et al. [10] prepared Fe-based alloy coating on 42CrMo by laser cladding, and researched the element distribution, microstructure and properties. The result revealed that the coating microhardness was three times higher than the steel substrate, the wear rate was half of the substrate, and the corrosion resistance was also higher. Li et al. [11] fabricated Fe-Cr alloy coating on Fe substrate using laser cladding and found that pearlitic structure appeared in the transitional area.

In conclusion, current research about laser cladding Fe-based alloy coating was concentrated on the effects of element addition, laser power and scanning velocity on coating microstructure and properties. However, systematic research on coating shear strength and wear properties was rarely reported. In some service environment, the coatings suffer severe shear stress accompanied by wear friction. The shear strength and properties should be researched, and the relationship between the microstructure, microhardness, shear behavior and wear properties deserve to be investigated. In this work, Fe-based alloy coatings were fabricated by laser cladding, and the microstructure, shear strength and wear properties were discussed.

2. EXPERIMENTAL PROCESS

2.1. Preparation of the coating

Commercial Fe-based alloy powder was adopted as the raw material fabricated by the gas atomization method.

* Corresponding author. Tel.: +86 13862689910;
fax: +86 051983972012. E-mail: *010640@jscc.edu.cn* (L. Xie)

The powder was sieved to control the particle size in the range of 50 – 150 μm. The nominal composition was listed in Table 1. 25Cr2Ni4MoV steel plates with a size of 100 × 100 × 40 mm were used as the substrate. Before laser cladding, the substrate was cleaned with a degreaser and deionized water. Then the substrate and powder were dried in an oven at 120 ℃ for 30 minutes, benefiting for preventing the agglomeration and improving the flowability. A 5 kW TJ-HLT5000 type continuous-wave CO_2-laser system was adopted to fabricate the coatings. High purity Argon gas was used as the protective gas during the cladding process to prevent the oxidation of coatings. The laser cladding parameters were listed in Table 2.

Table 1. Compositions of Fe-based alloy powder

Element	Fe	Cr	Ni	C	Mn	Mo	V	Si	B	O
wt.%	Bal.	17.2	2	0.15	0.25	1.63	0.1	1	0.92	0.05

Table 2. Parameters of laser cladding

Substrate	25Cr2Ni4MoV
Spot diameter	4 mm
Distance	360 mm
Feeding rate	220 – 224 g/min
Scanning speed	6 mm/s
Laser power	2000 W
Protecting gas	Ar

2.2. Specimen characterization

The prepared coatings were wire-electrode cut into square specimens with size of 10 mm × 10 mm and were hot mounted for subsequent analysis. Then the specimens were grinded orderly by sandpaper of 400#, 600#, 1000#, 1500# and 2000#. After that, specimens were polished to mirror the surface using diamond powder of 2 μm and 1 μm. XRD (X-ray diffraction) equipment (Rigaku 2550, Japan) was used to analyze the phase structure of Fe-based alloy powder. The scanning velocity, step size was 2θ/min and 0.02°, respectively. FSEM (field emission scanning electron microscopy, Mira 4, Tescan) was employed to investigate the microstructure of powder and the coatings before and after the wear friction test. EDS (Energy Disperse Spectroscopy, Oxford) was applied to examine the element distribution of the coatings. Vickers hardness tester was utilized to study the microhardness in various areas of coatings and substrate. The load and loading time were 5 kg and 15 s, respectively. At least 10 microhardness values were examined at every point, and the average was adopted as its final microhardness value. A reciprocating friction wear testing machine (HRS-2M, Zhongkekaihua, Lanzhou) was applied to research the wear performance of coatings and substrate. The friction load, reciprocating distance, friction time and repeating times were 20 N, 5 mm, 30 mins and 3, respectively. GCr15 steel balls with a diameter of 6 mm were utilized as the counterpart. Representative data and curves were used as the final friction results of specimens. A universal mechanical testing machine (Instron3369, America) was employed to study the mechanical properties of the coatings. The loading velocity of shear stress was 2 mm/min. Every specimen was tested at various locations to improve the accuracy of coating shear strength.

3. RESULTS AND DISCUSSIONS

3.1. Morphology and phase structure of the powder

Fig. 1 exhibits the cross-sectional morphology of the Fe-based alloy powder. From Fig. 1, most powder particles display round and ellipsoidal shapes. This kind of powder shape will benefit transporting and laser cladding because the flowability was excellent and the melting degree was uniform. The powder size distributes from 50 to 120 μm, and the average is 110 μm.

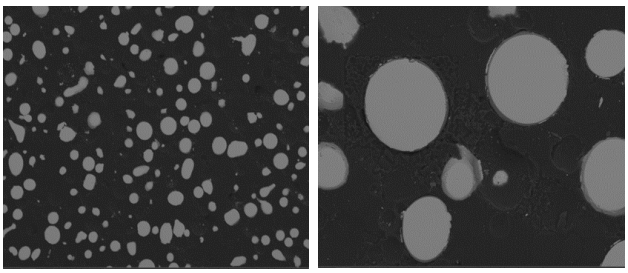

a b

Fig. 1. SEM images of Fe-based alloy powders: a – panorama; b – local magnification image

Fig. 2 shows the element map distributions of Fe-based alloy powder. From the pictures, the Fe, Cr and Ni elements uniformly distribute inside the powder particle, which indicates the powder obtains a homogeneous composition, beneficial to synthesize a high-quality coating.

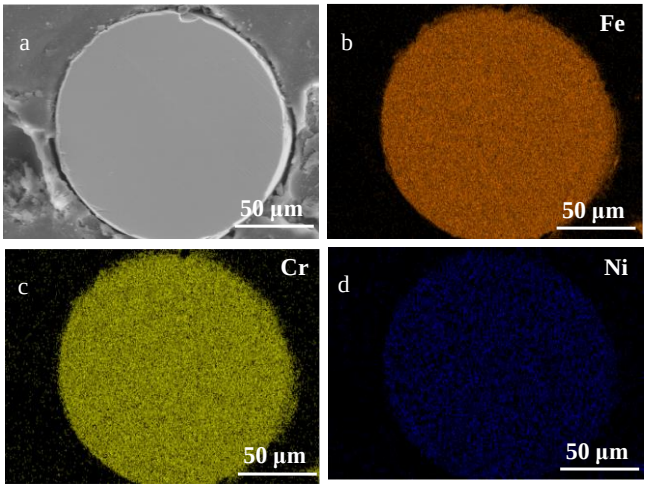

Fig. 2. Element map distributions of Fe-based alloy powder: a – selected area; b – Fe element; c – Cr element; d – Ni element map distributions

Fig. 3 displays the XRD pattern of Fe-based alloy powder. From Fig. 3, the dominant phase of the coating is $FeCr_XNi_Y$, and the crystal planes are (110), (200), (211), (220), respectively. Several Fe_3Ni_2 phases exist with crystal planes of (111) and (200). It can be deduced that the Fe-based alloy powder is primarily composed of the compounds Fe, Cr and Ni, which are mostly nanocrystalline and dendrite crystalline due to the rapid cooling velocity of melting powder particles during the laser cladding process. The formed fine crystalline will improve the microhardness and wear resistance [12, 13].

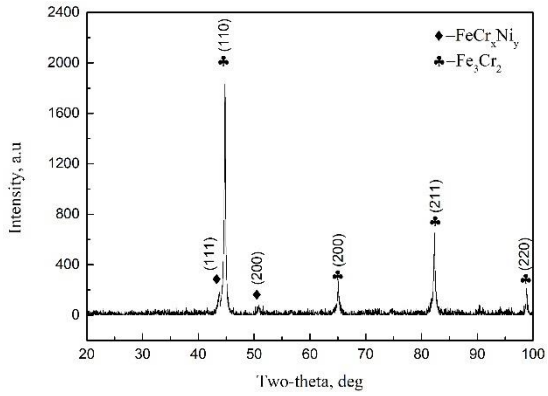

Fig. 3. XRD patterns of Fe-based alloy powders

3.2. Microstructure and element distribution of the coatings

Fig. 4 exhibits the interface morphology and element distribution between the coating and substrate. It can be seen that the bonding between coating and substrate is tight, and Fe, Cr, Ni and Mo uniformly distribute in the coating. This indicates the element distribution of raw material didn't change during laser cladding. The EDS map scanning of Fig. 4 e shows that the O element rarely distributes in the coating, and the content is lower than 1.0 wt.% as tested. The O element in the coating is close to that in the raw powder, implying that the inert gas can effectively prevent alloy element oxidation and reduce the impurity content of the coating.

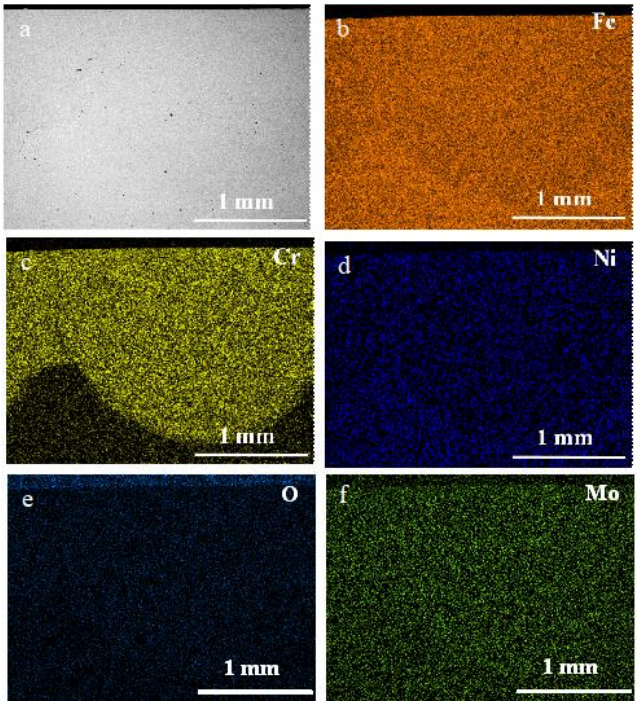

Fig. 4. Morphology and element map distributions of the interface between Fe-based alloy coating and 25Cr2Ni4MoV matrix: a – SEM image; b – Fe; c – Cr; d – Ni; e – O; f – Mo element map distributions

Fig. 5 presents the microstructure of the laser cladded Fe-based alloy coating. From Fig. 5 a, the coating and substrate obtain an excellent bond, yet a part exhibits several pores which can be due to the CTE (coefficient of thermal expansion) difference between coating and substrate during the laser cladding.

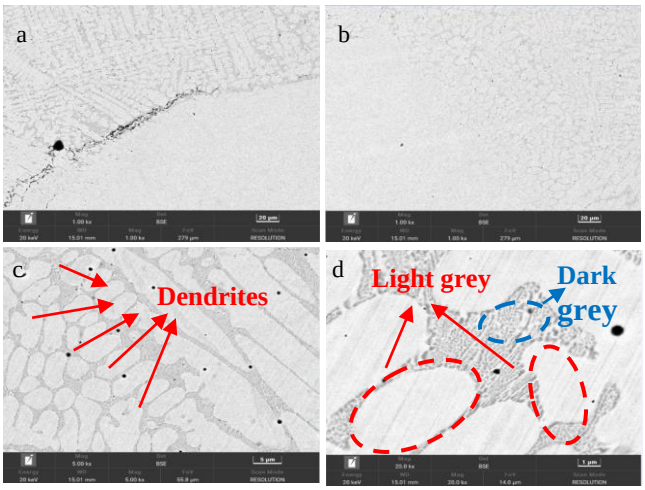

Fig. 5. SEM images of Fe-based alloy coatings prepared by laser cladding: a, b – morphologies at interfaces; c, d – local magnification images of Fe-based alloy coating near the bottom of the molten pool

From Fig. 5 b, metallurgical bonding exists in several regions of the interface, indicating the bonding between coating and substrate reached the atomic level. The coating near the interface is magnified as exhibited in Fig. 5 c, it can be seen the cladded coating in the bottom of the weld pool shows the typical dendrite crystalline, which is composed of two phases, light grey and dark grey. The typical microstructure of laser cladded coatings is due to the high temperature gradient during laser cladding. As magnified in Fig. 5 d, the dark grey phase is composed of fine crystalline.

Fig. 6 exhibits the element mapping distribution of the laser cladded Fe-based alloy coating. From Fig. 6 c and f Cr and Mo elements mainly distribute in the dark grey phase. From Fig. 6 b and d Fe and Ni elements mostly distribute in the light grey phase. This result indicates that the dendrite crystalline is composed of Fe and Ni alloy, and other components are mainly Cr and Mo alloys. During the laser cladding process, the substrate and powder form a melting pool with superhigh temperature, then rapidly cool down as the laser head moves [14, 15].

The high cooling velocity leads to the coarse columnar crystalline of metal elements like Fe and Ni, and gradually grows up to the crystallographic axis. The crystallographic axis crystallizes accompanied by producing latent heat to the liquid phase, which leads negative temperature gradient along the direction perpendicular to the crystallographic axis. Then the second crystallographic axis will grow on the first crystallographic axis, exhibiting dendritic shape. At the same time, the Cr and Mo alloy fill the gaps between the dendrite crystalline [7, 11].

Fig. 7 displays the inner morphology of the laser cladded Fe-based alloy coating. From Fig. 7 a and b, the coating obtains a compact microstructure, and a small number of pores are found, which can be ascribed that during the laser cladding, some low melting point material evaporates from the melting pool and leads to several bubbles [16, 17].

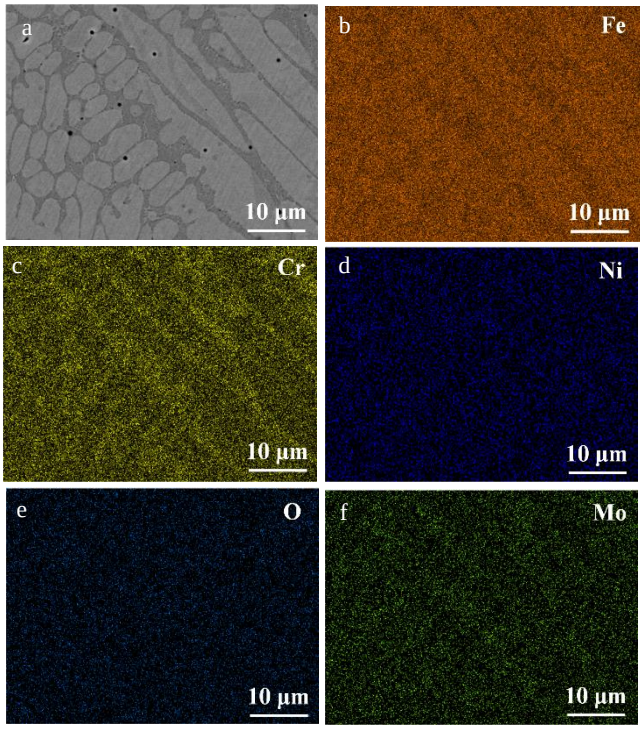

Fig. 6. Element map distributions of Fe-based alloy coatings prepared by laser cladding: a – SEM image of the selected area; b – Fe; c – Cr; d – Ni; e – O; f – Mo element map distributions

A part of the bubbles can't escape from the melting pool in time, and remain in the formed coating, turning into the pores. The inner coating is magnified in Fig. 7 c and d, revealing a large amount of dendrite crystalline generated which is the typical microstructure of laser cladded coating.

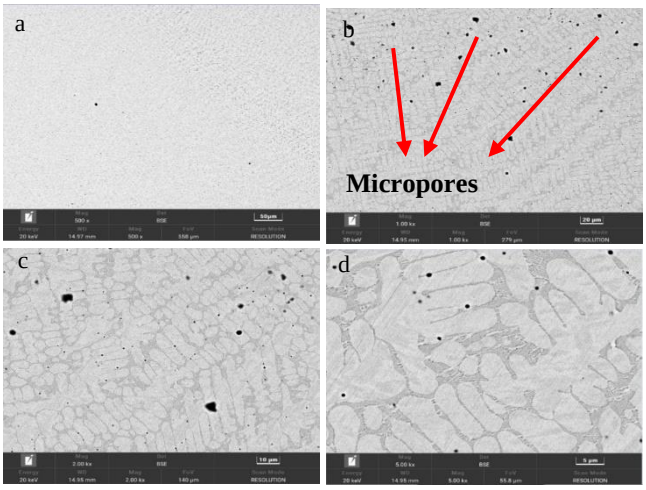

Fig. 7. SEM images of middle part of Fe base alloy coatings prepared by laser cladding: a – panorama; b – micro-pores; c, d – dendritic crystals in the coating

3.3. Mechanical properties of laser cladded Fe-based alloy coating

3.3.1. Microhardness

Melting pools with a big thickness will generate during the laser cladding, which means several large heat-affected zones will appear at the interface between coating and substrate due to the high energy of the laser. The microhardness in the matrix zone, heat affected zone and coating zone are exhibited in Fig. 8. It can be seen that there is a big difference in the microhardness in various zones, and the coating zone obtains the highest microhardness among the three zones. It can be inferred that the solid solution formed by Fe, Cr and Ni alloy significantly increased the coating microhardness and strength, especially the Fe-based solid solution [18, 19]. The heat affected zone is located in the transitional area of the coating and substrate, so the microhardness ranges between the above two zones. The Fe, Cr and Ni alloy solid solution greatly increase the coating hardness relative to the steel substrate. Moreover, the cooling speed is higher in the coating than in the heat affected zone and matrix zone due to the distance from the laser head to the matrix.

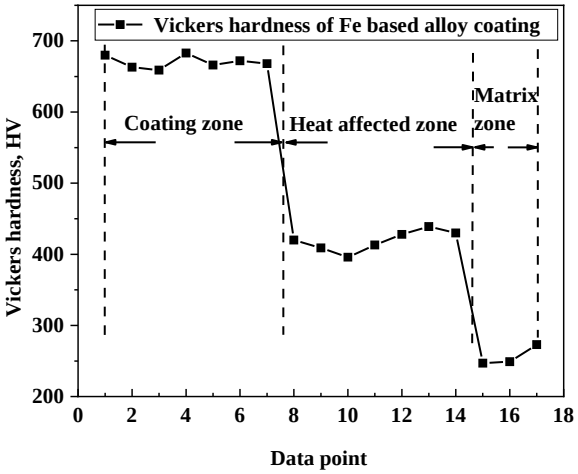

Fig. 8. Vickers hardness values of Fe-based alloy coatings prepared by laser cladding

3.3.2. Shear strength

The shear strength experiment process was demonstrated in Fig. 9. The machined coating sample was sheared to fracture, and shear strength-displacement curves of the sheared parts are presented in Fig. 10.

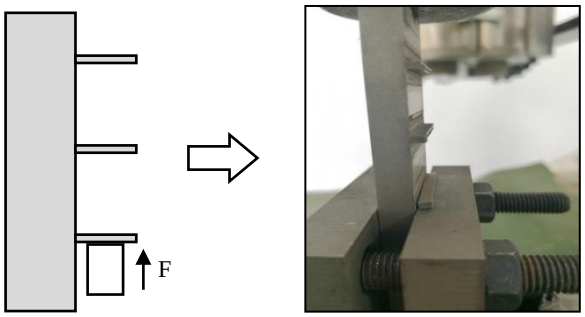

Fig. 9. Shear resistance test of laser cladding Fe-based alloy coatings

From Fig. 10, all the curves exhibit a typical brittle fracture characteristic, and the average shear strength reaches up to 280.83 MPa. The shear strength represented by line 1 is lower than the other two, which should be due to microstructure difference in various areas. Additionally, the porosity is also an influence factor in the difference in shear strength because the area obtaining more pores will

display a lower resistance to shear stress than those with less pores.

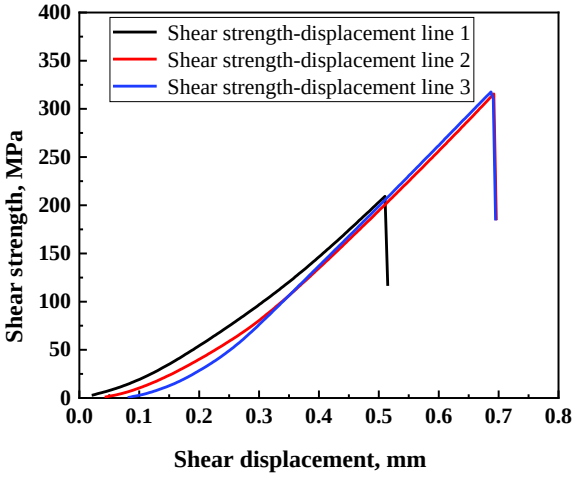

Fig. 10. Shear strength-displacement curves of Fe-based alloy coatings prepared by laser cladding

Fig. 11 exhibits the shear fracture surfaces of laser cladded Fe-based alloy coatings. From Fig. 11 a and b, a large number of dimples appeared in the fracture area, meaning the shear fracture mainly occurred in the form of detaching of particles or grains. Several river-like textures and brittle fracture can be seen in Fig. 11 c and d, indicating the typical intracrystalline fracture characteristic which can provide high strength for the coating.

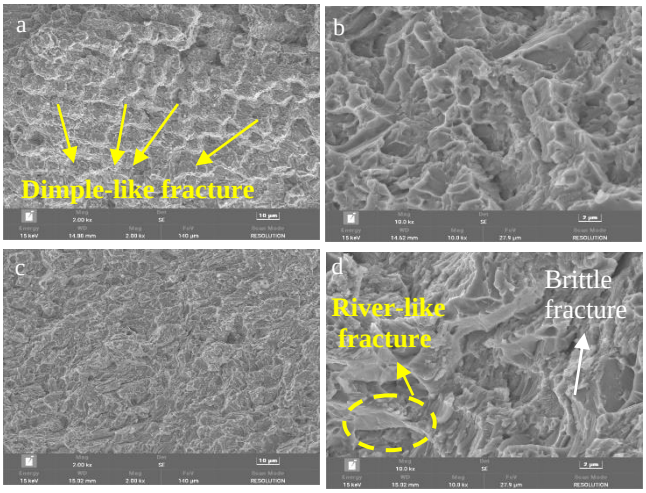

Fig. 11. SEM images of shear fracture surfaces of laser cladded Fe-based alloy coatings: a – panorama; b – high magnification image; c – panorama; d – high magnification image

3.3.3. Wear behavior

The friction curves of laser cladded Fe-based coatings and substrate are displayed in Fig. 12. It can be seen that the friction curves of the coatings exhibit a stable and gentle trend, the average of friction coefficient is 0.45 ± 0.01. The 25Cr2Ni4MoV substrate shows a unstable and fluctuant trend, the average of friction efficient is 0.60 ± 0.01. From the result, laser cladded Fe-based alloy coating obtains a better wear resistance than 25Cr2Ni4MoV substrate and can be applied in the universal industrial field for surface protection.

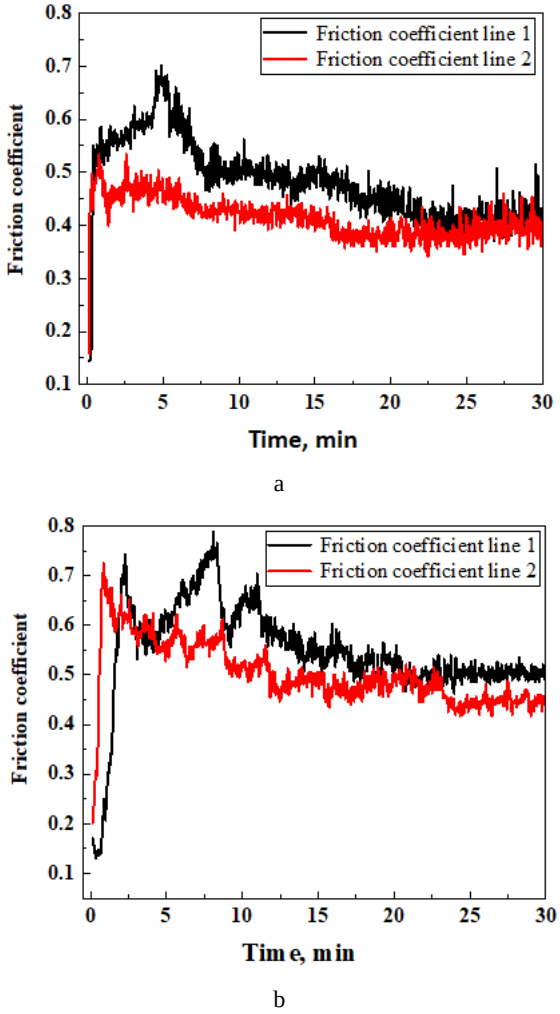

Fig. 12. Friction-time coefficients: a – laser cladded Fe-based alloy coatings; b – 25Cr2Ni4MoV matrix

Fig. 13 exhibits the wear track of the coatings and substrate. From the picture, the average wear track depth of the coatings was 26 ±3 μm, and that of the substrate is 39 ± 3 μm. The average wear track depth of the coating is smaller than the substrate, mainly because the coating obtains higher microhardness than the substrate, and the higher microhardness, the stronger resistance to the needle tip it owns. Generally speaking, the deeper the wear track depth is, the weaker wear resistance it owns. Therefore, the laser cladded Fe-based alloy coating obtains better wear resistance than the substrate. The average wear volume of the laser cladded Fe-based coating is approximately 0.066615 m^3, and that of the substrate is about 0.13085 m^3. In other words, the wear rate of the coating is about half of the substrate, indicating the coating obtains better wear properties. This result agrees with the above conclusion.

Fig. 14 exhibits the friction surface morphology of the substrate and coatings. From Fig. 14 a and b, a large quantity of coarse broken particles appeared on the substrate surface, and several huge particles and big cracks can be found. Combining with the above microhardness data, it's obvious that the substrate microhardness was low, hence microcracks were generated when the shear stress exceeded the ultimate strength during the wear experiment. As the wear friction proceeded, the microcracks gradually increased, finally a large quantity of bulk material broke

off, and a lot of fine particles were produced, which was the typical abrasive wear mechanism morphology [20, 21].

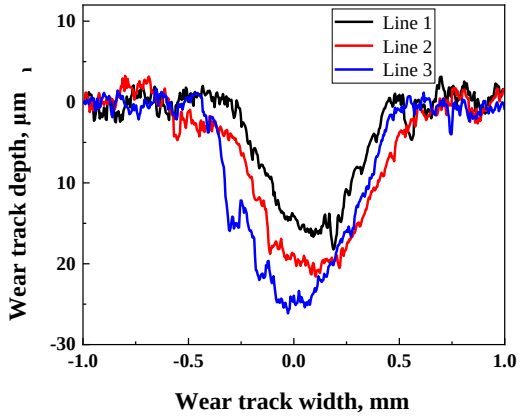

a

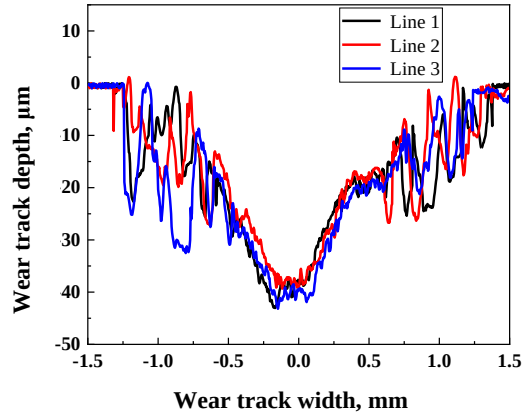

b

Fig. 13. Wear track profiles: a – laser cladded Fe-based alloy coatings; b – 25Cr2Ni4MoV matrix

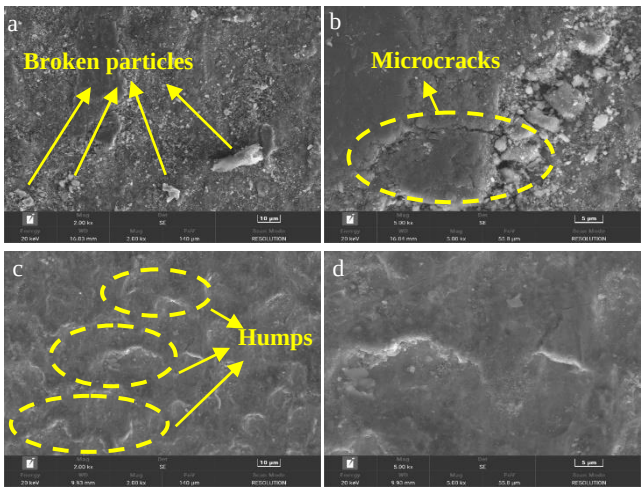

Fig. 14. SEM morphologies of worn surfaces: a – matrix ×2000; b – matrix ×5000; c – Fe-based alloy coating ×2000; d – Fe-based alloy coating ×5000

From Fig. 14 c and d, the coating surface was relatively smooth, and many lamellar humps were found. It can be inferred that the coating microhardness was super high, meaning the resistance to the counterpart was strong. Therefore, the friction load can hardly exceed the resistance, indicating the microcracks can't easily generate. As the wear friction continued, the reciprocating motion of friction load led to fatigue stress which caused local delamination and several humps can be found resulting from it.

4. CONCLUSIONS

1. Metallurgical bonding was formed at the interface of laser cladded Fe-based alloy coating and 25Cr2Ni4MoV substrate. The coating exhibited typical dendrite morphology and was composed of two phases displaying light grey and dark grey, respectively.
2. The microhardness of the cladding coating zone is markedly higher than the transitional zone and substrate. The shear strength-displacement curve exhibits typical brittle fracture characteristics, and the average shear strength reached 280.83 MPa.
3. The friction coefficient, wear track depth and average wear volume of laser cladded Fe-based alloy coating are 0.45 ± 0.01, 26 ± 3 μm and 0.066615 m^3, respectively.
4. The wear resistance of laser cladded Fe-based alloy coating is much higher than 25Cr2Ni4MoV substrate, indicating the coating can greatly protect steel substrate from wear friction.

Acknowledgments

This work was supported by Natural Science Foundation of Hunan Province of China (Grant No. 2021JJ50025), Key Research and Development Program of Hunan Province (2022GK2030), Natural Science Project of Jiangsu Urban and Rural Construction Vocational College (XJZK22009/206).

REFERENCES

1. **Zhang, P., Yan, H., Yao, C., Li, Z., Yu, Z., Xu, P.** Synthesis of Fe-Ni-B-Si-Nb Amorphous and Crystalline Composite Coatings by Laser Cladding and Remelting *Surface and Coatings Technology* 206 2011: pp. 1229 – 1236. https://doi.org/10.1016/j.surfcoat.2011.08.039
2. **Zhu, Q., Qu, S., Wang, X., Zou, Z.** Synthesis of Fe-based Amorphous Composite Coatings with Low Purity Materials by Laser Cladding *Applied Surface Science* 253 2007: pp. 7060 – 7064. https://doi.org/10.1016/j.apsusc.2007.02.055
3. **Reddy, L., Preston, S.P., Shipway, P.H., Davis, C., Hussain, T.** Process Parameter Optimisation of Laser Clad Iron Based Alloy: Predictive Models of Deposition Efficiency, Porosity and Dilution *Surface and Coatings Technology* 349 2018: pp. 198 – 207. https://doi.org/10.1016/j.surfcoat.2018.05.054
4. **Zhang, H., Zou, Y., Zou, Z., Wu, D.** Microstructure and Properties of Fe-based Composite Coating by Laser Cladding Fe-Ti-V-Cr-C-CeO_2 Powder *Optics & Laser Technology* 65 2015: pp. 119 – 125. https://doi.org/10.1016/j.optlastec.2014.06.016
5. **Li, Q., Lei, Y., Fu, H.** Laser Cladding in-situ NbC Particle Reinforced Fe-based Composite Coatings with Rare Earth Oxide Addition *Surface and Coatings Technology* 239 2014: pp. 102 – 107.

https://doi.org/10.1016/j.surfcoat.2013.11.026

6. **Cao, Y.B., Hong, T., Hu, C.S., Meng, Q.X., Liu, Q.** In-situ Formation Behavior of NbC-reinforced Fe-based Laser Cladding Coatings *Materials Letters* 147 2015: pp. 61 – 63. https://doi.org/10.1016/j.matlet.2015.02.026
7. **Lu, J.Z., Cao, J., Lu, H.F., Zhang, L.Y., Luo, K.Y.** Wear Properties and Microstructural Analyses of Fe-based Coatings with Various WC Contents on H13 Die Steel by Laser Cladding *Surface and Coatings Technology* 369 2019: pp. 228 – 237. https://doi.org/10.1016/j.surfcoat.2019.04.063
8. **Luo, X.X., Cao, J., Meng, G.H., Chuan, Y.Y., Yao, Z.J., Xie, H.** Systematical Investigation on the Microstructures and Tribological Properties of Fe-Al Laser Cladding Coatings *Applied Surface Science* 516 2020: pp. 146121. https://doi.org/10.1016/j.apsusc.2020.146121
9. **Zhao, L.Z., Zhao, M.J., Li, D.Y., Zhang, J., Xiong, G.Y.** Study on Fe–Al–Si in situ Composite Coating Fabricated by Laser Cladding *Applied Surface Science* 258 2012: pp. 3368 – 3372. https://doi.org/10.1016/j.apsusc.2011.09.057
10. **Ju, J., Zhou, Y., Kang, M., Wang, J.** Optimization of Process Parameters, Microstructure, and Properties of Laser Cladding Fe-Based Alloy on 42CrMo Steel Roller *Materials* 11 2018: pp. 30360401. https://doi.org/10.3390/ma11102061
11. **Li, Y.J., Dong, S.Y., Yan, S.X., Liu, X.T., He, P., Xu, B.S.** Microstructure Evolution during Laser Cladding Fe-Cr Alloy Coatings on Ductile Cast Iron *Optics & Laser Technology* 108 2018: pp. 255 – 264. https://doi.org/10.1016/j.optlastec.2018.07.004
12. **Emamian, A., Corbin, S.F., Khajepour, A.** Effect of Laser Cladding Process Parameters on Clad Quality and in-situ Formed Microstructure of Fe-TiC Composite Coatings *Surface and Coatings Technology* 205 2010: pp. 2007 – 2015. https://doi.org/10.1016/j.surfcoat.2010.08.087
13. **Wang, C., Zhang, S., Zhang, C.H., Wu, C.L., Zhang, J.B., Abdullah, A.** Phase Evolution and Wear Resistance of in situ Synthesized V8C7 Particles Reinforced Fe-based Coating by Laser Cladding *Optics & Laser Technology* 105 2018: pp. 58 – 65. https://doi.org/10.1016/j.optlastec.2018.02.019
14. **Cropper, M.D.** Thin Films of AlCrFeCoNiCu High-Entropy Alloy by Pulsed Laser Deposition *Applied Surface Science* 455 2018: pp. 153 – 159. https://doi.org/10.1016/j.apsusc.2018.05.172
15. **Ye, X.Y., Ma, M.X., Cao, Y., Liu, W.J., Ye, X.H., Gu, Y.** The Property Research on High-entropy Alloy AlxFeCoNiCuCr Coating by Laser Cladding *Physics Procedia* 12 2011: pp. 303 – 312. https://doi.org/10.1016/j.phpro.2011.03.039
16. **Jin, G., Cai, Z.B., Guan, Y.J., Cui, X.F., Liu, Z., Li, Y., Dong, M., Zhang, D.** High Temperature Wear Performance of Laser-Cladded FeNiCoAlCu High-Entropy Alloy Coating *Applied Surface Science* 445 2018: pp. 113 – 122. https://doi.org/10.1016/j.apsusc.2018.03.135
17. **Ni, C., Shi, Y., Liu, J., Huang, G.Z.** Characterization of Al0.5FeCu0.7NiCoCr High-Entropy Alloy Coating on Aluminum Alloy by Laser Cladding *Optics & Laser Technology* 105 2018: pp. 257 – 263. https://doi.org/10.1016/j.optlastec.2018.01.058
18. **Chen, J.M., Guo, C., Jian, S.** Microstructure and Tribological Properties of Laser Cladding Fe-based Coating on Pure Ti Substrate *Transactions of Nonferrous Metals Society of China* 22 2012: pp. 2171 – 2178. https://doi.org/10.1016/s1003-6326(11)61445-3
19. **Zhou, S., Xu, Y., Liao, B.** Effect of Laser Remelting on Microstructure and Properties of WC Reinforced Fe-based Amorphous Composite Coatings by Laser Cladding *Optics & Laser Technology* 103 2018: pp. 8 – 16. https://doi.org/10.1016/j.optlastec.2018.01.024
20. **Zhang, H., Pan, Y., He, Y.Z.** Synthesis and Characterization of FeCoNiCrCu High-Entropy Alloy Coating by Laser Cladding *Materials & Design* 32 2011: pp. 1910 – 1915. https://doi.org/10.1016/j.matdes.2010.12.001
21. **Zhang, H., Pan, Y., He, Y.Z., Jiao, H.S.** Microstructure and Properties of 6FeNiCoSiCrAlTi High-Entropy Alloy Coating Prepared by Laser Cladding *Applied Surface Science* 257 2011: pp. 2259 – 2263. https://doi.org/10.1016/j.apsusc.2010.09.084